Materials Chemistry and Physics 256 (2020) 123716

Contents lists available at ScienceDirect

Materials Chemistry and Physics

journal homepage: www.elsevier.com/locate/matchemphys

Ultra-fine beta SiC nanowires Isothermally converted from high activated silica by Carbothermic Reduction and Carburization at low temperature

Engin Kocaman [a,*], Fatih Çalışkan [b]

[a] Zonguldak Bulent Ecevit University Faculty of Engineering, Department of Metallurgical and Materials Engineering, İncivez, 67100, Zonguldak, Turkey
[b] Sakarya University of Applied Sciences, Faculty of Technology, Department of Metallurgical and Materials Engineering, 54187, Sakarya, Turkey

HIGHLIGHTS

- Ultra-fine β-SiC nanowires were synthesized via a carbothermic reduction–carburization process.
- Improvement in the efficiency of the processes was achieved by a mechanochemical preparation.
- The synthesis reactions were carried out at relatively low temperatures.
- Monophasic β-SiC powder was successfully synthesized at 1475 °C for 4 h.
- The SiC superfine crystallites with 50–100 nm in diameter were obtained.

GRAPHICAL ABSTRACT

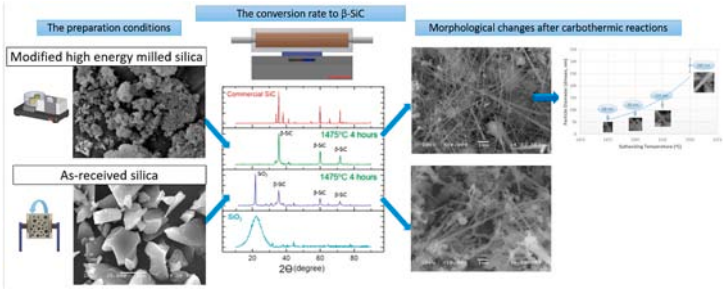

ARTICLE INFO

Keywords:
Carbide
Nanowire
Carbothermal reduction carburization
Synthesis
Pre-mechanical activation

ABSTRACT

This work was focused primarily on the investigation of the parameters effecting the formation of β-SiC and their crystallite diameter. Previous works revealed that the preparation of silica used as a precursor was the key factor on the resulting particle features. Therefore, the work aimed to achieve obtaining ultrafine silica precursor with superfine crystallites at relatively low temperatures. In the result, a clear difference was observed between the finally obtained SiC powders in terms of conversion and particle morphology according to the preparation process. The use of a modified high energy ball milling system resulted in a considerable reduction in the size of the starting particle's diameter (>100 nm). The FTIR transmission spectra of the yielded nanowires confirmed the SiC composition with the peak near 950 cm−1, which represents the LO stretching Si–C bond. The precursor preparation process improved the efficiency of Carbothermic Reduction and Carburization process used in the synthesis of SiC nanowires. The XRD findings indicated that all the precursors consisted of only amorphous silica, and the modified high energy ball milling system thermodynamically supported the crystal to amorphous conversion. The SEM micrographs revealed that the SiC nanowires had diameters of 50–100 nm with hundreds of microns in length. The SiC nanowire composed of ultrafine crystalline cubic SiC in beta form. As a result, the silica conversion to silicon carbide was successfully completed at a faster reduction rate and relative lower temperature (1475 °C for 4 h).

* Corresponding author.
E-mail addresses: enginkocaman@beun.edu.tr (E. Kocaman), enginkocaman@gmail.com (E. Kocaman), fcaliskan@subu.edu.tr (F. Çalışkan).

https://doi.org/10.1016/j.matchemphys.2020.123716
Received 24 November 2019; Received in revised form 23 June 2020; Accepted 16 August 2020
Available online 21 August 2020

1. Introduction

Silicon carbide is very important ceramic material due to its superior properties such as high hardness and strength, excellent resistance to oxidation and corrosion, low thermal expansion coefficient and high heating transfer capabilities [1,2]. In addition, the whisker form of SiC can be used as a reinforcement in composite ceramics due to increased room and high-temperature fracture toughness [3]. This material is mostly used in the industrial area each as electrical industries, high-temperature ceramic devices and as reinforcement for ceramic composites [4–7]. These have excellent chemical properties accounting strong bonds between carbon atoms and such cations as Si, B, Ti, etc. [8]. As an important product, the cost of SiC widely depends on its purity and some studies are trying to reduce cost nowadays [9]. The silicon carbide powders can be produced by many methods. Four basic methods are used in the synthesis of silicon carbide, namely; (1) direct carbonization, (2) chemical vapor deposition, (3) sol-gel method, (4) carbothermic reduction [8,10].

Carbothermic reduction and carburizing (CRC) are generally known as easy methods to produce silicon carbide powders [11]. It is an economically attractive production route because of the use of inexpensive various carbon and low-cost silica sources chosen as the starting materials [12,13] The Acheson process which was generated from the CRC method is the most popular method nowadays [10,14].

Silicon carbide was synthesized in an appropriate atmosphere by carbothermic reduction and carburizing of silica (SiO_2) according to the overall reactions. Two silicon carbide modifications can be produced depending on the reaction temperature, namely, α-SiC occurred above 2400 °C and β-SiC formed between 1400 and 2000 °C. Reaction one had an endothermic character with $\Delta H^o_{298} = 618.5$ kJ and the SiC formation began at a temperature about 1500 °C. This result is determined with the Gibbs free energies of each component in the equilibrium conditions.

$$SiO_{2(s)} + 3C_{(s)} \rightarrow SiC_{(s)} + 2CO_{(g)} \quad (1)$$

Reaction (1) is believed to be going by two steps of the CRC process. First, until 1500–1600 °C is reached, the reactions (2) and (3) proceeded. The reaction is carried out under 1500 °C or lower as a gas-solid ($SiO_{(g)}$-$C_{(s)}$), favouring powder formation. Reaction (2) is extremely endothermic and it is needed to elevate the temperature. Reaction (3) is of exothermic character and it is quite important for β-SiC nanopowder formation.

$$SiO_{2(s)} + C_{(s)} \rightarrow SiO_{(g)} + CO_{(g)} \quad (2)$$

$$SiO_{(g)} + 2C_{(s)} \rightarrow SiC_{(s)} + CO_{(g)} \quad (3)$$

Just above 1600 °C, the dominated reaction is believed to be a $SiO_{(g)}$+$CO_{(g)}$ gas-gas reaction, favouring whisker formation. Acting as catalysts, the transition metals (especially Fe, Co, Ni) promote in the gas-gas reaction to form whiskers [8,10,11,15,16]. As a consequence, the SiC yield of carbothermal reaction depends on such parameters as non-stoichiometric silicon-carbon ratio, process temperature, and high-pressure inert atmosphere [17]. In addition, enough time is thermodynamically needed to complete the transformation reaction.

The SiC powder obtained by carbothermal reduction and carburization process is in the form of large chunks [18]. The carbothermic reactions (reducing/carburizing) require a high temperature of synthesis [19]. The conventional way of producing SiC powder provides the non-uniform particle morphology [20]. The obtained powder is generally included fine particles, agglomerates, coarse particles, which are due the high temperature of synthesis [21,22].

The CRC method can be used for synthesis of nanoscale whiskers or rods [23,24]. In this case, often the product is not a uniformly submicron SiC powder. The SiC powder produced by commercial CRC process is extremely hard, but fine. To obtain a superfine powder, the milling of this material down to a submicron powder requires a high exertion. Frequently, the conversion is not complete [18,25].

Other production methods of super fine and pure SiC powders (such as sol-gel [26], xerogels [27], reaction milling [4], microwave heating [28], direct pyrolysis of RH [29], CVD [30], polyethylene pyrolysisi etc.) are less suitable for mass production due to low efficiency, high agglomeration and high-cost [31]. Thus alternative techniques to improve the carbothermal reduction process are of interest.

With the further development of the milling of the starting materials, it creates new possibilities for the mechanochemical synthesis of silicon carbide powders and the time for the formation of the SiC is reduced [4]. After a certain milling time, as the particle size decreases, during which the components are thoroughly mixed, while the number of chemically active defect sites increases, the energy barrier required for SiC nuclei formation is significantly reduced and the conversion reaction progresses [4,31,32].

Limited studies reported on improvements in the quality and yield of β-SiC nanowires. There is the large supply-demand gap. Therefore, further investigations are necessary to improve and optimize the synthesis of nanocrystalline SiC via the CRC method. In addition, extensive research has been conducted to develop a method for lowering the reaction temperature of the carbotermal reduction method [25].

The objective of this present work is to carry out the efficient solid-state synthesis of SiC by the CRC process. For this reason, this experimental research aims to produce the monophasic ultra-fine β-SiC nanowires by carbothermic reduction and carburizing of mechanically high activated silica with carbon black in a tube furnace at the comparatively low temperatures. The conversion SiC from silica by the CRC process was achieved accompanied by a considerable decrease in the plateau temperature. The modified high energy ball milling process for the precursor improved the efficiency of the CRC process used in the synthesis of nanocrystalline SiC. The formation of silicon carbide was investigated and characterized using conventional analytic methods (SEM, EDS, XRD, FTIR). In addition, the technological parameters were optimized to reach cost-effective CRC process and increase the purity of final SiC products.

2. Materials and method

In this method, the properties of the starting materials are important to obtain the silicon carbide in terms of cost-effectiveness and purification. Two basic materials, quartz mineral as Si source and carbon as a reducing agent, were used in this study. Quartz mineral was received from Ege Kimya Company (Turkey) whose properties are given in Table 1. Carbon black was received from CABOT (coded as Vulcan XC 72), 99.7% purity having a specific surface area of 110 $m^2\ g^{-1}$. Also, a commercial SiC (>98% purity, 40 μm) was supplied from EGE-Nanotek Company to reveal the seeding effect.

Quartz mineral was mixed with carbon black just above the stoichiometric ratio according to the reaction (1). The mixture was ground three times for 5 min and milled with a modified high energy ball milling system (MHEM) for 24 h at room temperature in order to have a homogeneous mixture. Some compositions were only mixed with the CPM (not ground) to investigate the grinding effect on powder morphology. The carbothermic reduction and carburizing reactions were carried out using a tube furnace (Protherm PTF Series) under the flowing argon atmosphere (99.999% purity from The Linde Group, Turkey). More than one type of temperature procedures were used to heat the compositions. The implemented temperature range was chosen to expand upon previous research on the carbothermal reduction method. The mixture powders were then transferred to hot zone of a horizontal alumina tubular furnace using alumina crucible. After the carbothermal

Table 1
Properties of quartz mineral supplied by Ege Kimya A.S., Turkey.

Main phase (wt%)	Impurity (wt%)	Metallic Fe (wt%)	Density g/cm^3
SiO_2 (min 98%)	Max. 2%	Max. 0.05	2.65

reduction, the product was heated in an ash furnace to burn the residual carbon out in an air atmosphere at 900 °C for 2 h. All powder compositions used in this study are given in Table 2.

The powder morphology was analyzed using a scanning electron microscope (SEM, JEOL 6060LV). The transformation characteristics were determined by X-ray diffraction (XRD) analysis using a Rigaku D/MAX 2000/PC (Japan) X-ray diffractometer with Cu-Kα radiation and the phase identification was performed using X'Pert High Score software. The particle size measurement on SEM micrographs was carried out by the Clemex Vision Lite program.

The measurement of particle size distribution of the quartz mineral was made by using a Mastersizer 2000 (Malvern Instruments, Worcs., UK). The particle size distribution can be seen in Fig. 1. The particle size analyser showed that the average particle size was 15 μm. It could be accepted as a monomodal distribution. There was a minor amount of powder under 1 μm. That is to say, the starting powder was in micro-size.

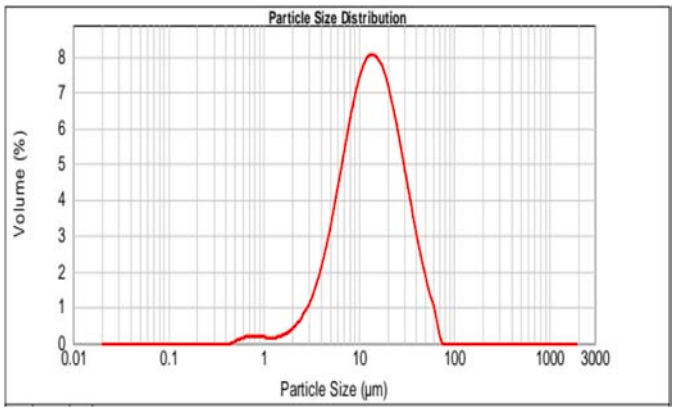

Fig. 1. Particle size distribution of quartz mineral.

3. Results and discussion

3.1. PXRD results

In this work, the effect of different experimental conditions such as temperature, duration, milling and composition parameters on the synthesis of SiC was investigated. Four different synthesis time of 1–4 h was chosen according to previous studies. Among ten samples, eight samples were ground by using both a modified ball milling developed by Caliskan et al. [33] and high energy milling systems about 24 h before sintering. The synthesis reactions were produced at the temperature ranging from 1475 to 1550 °C for 1–4 h.

3.1.1. PXRD analysis of starting powder after the MHEM process

The unreacted ultrafine silica nanoparticles were obtained after high energy milling. The XRD pattern of the SiO_2 product corresponds to amorphous state of silica (Fig. 2). The silica particles showed entirely the amorphous nature and XRD pattern similar to that observed in the previous investigations [34,35]. The powder diffraction pattern contains a very wide peak with maximum at $2\theta = 22°$. Further, the XRD pattern confirms the absence of any ordered crystalline structure.

Yves Fleming et al. explained that, the Si and O atoms are arranged differently even of the similar chemical composition. The difference in their crystal structure is reflected in their different diffraction patterns [36,37] -rays of an amorphous phase are scattered in many directions leading to a large bump distributed in a wide range in place of high intensity narrower peaks [38].

Tunça et al. and Mustafa Boyrazlı et al. reported that, if milling period is increased, all crystalline features in the XRD patterns gradually decrease. The prolonged milling time can be caused to decrease in peak lengths of the amorphous phases. During the milling process, the mechanical energy is transferred from structural irregularities [39,40]. The high energy milling stage of the starting powders is described by intensive plastic deformation of the particles at very high strain rate, formation of the high-density defects. In the early stages of ball milling, the average atomic level strain increases due to the increasing dislocations density. These sites due to the stored energy in the starting powders during the mechanical treatment are potential sites for the nucleation of new crystallites. Creation of fresh surfaces during the milling process is accepted to be one of the main sources of the reactivity [41–43].

In addition, a shrinkage appears in the XRD peak profile with regarding semi-stable amorphous phases after a mechanical milling [37]. In this study, it was considered that similar behaviour was carried out for the high energy milled silica.

Table 2
Powder compositions in experiments.

Experiment	Temperature (°C)	Time (hr.)	C/SiO_2	SiC (%)	Grinding
1	1550	4	1/3	–	+
2	1525	4	1/3	–	+
3	1500	4	1/3	–	+
4	1475	4	1/3	–	+
5	1475	3	1/3	–	+
6	1475	2	1/3	–	+
7	1475	1	1/3		+
8	1475	4	1/3	–	–
9	1475	4	1/3	10	+
10	1475	4	1/3	10	–

3.1.2. PXRD analysis after the CRC process

3.1.2.1. Time and temperature effects in the CRC reaction. The XRD patterns recorded for the powders synthesized by the CRC processing at 1475 for 1–4 h and at 1500–1575 °C for 4 h are shown in Fig. 3. In addition, as a reference, the XRD pattern of as-received commercial SiC powder is presented in Fig. 3.

The XRD patterns of commercial SiC and synthetic products obtained at 1475 °C for different reaction times are given in Fig. 3(a). It is obvious that longer sintering times enhance SiC formation. With increasing sintering time, the peak intensity of β-SiC increases while those of other phases decrease. As it is seen, the peak intensity of SiC sharply increases when the synthesis time changes from 1 to 4 h. As can be seen in Fig. 3a, the intensity of the peak of β-SiC for "1475 °C for 4 h" at 2θ of 71.84° has risen slightly; meanwhile the intensity of silica peaks decreased slightly compared to "1475 °C for 3 h". In the CRC reactions for >3 h at 1475 °C, no signal of the unreacted SiO_2 is observed. When the time reaches 4 h, almost all SiO_2 and C transform to β-SiC. Therefore, the synthesis of SiC needs sufficient sintering time and temperature. But, incremental in the plateau decreases the reaction time, ie. the time varies inversely with the temperature in a certain range. It is well-known that silicon carbide has two different crystalline forms: hexagonal α-SiC is a high-temperature form, while cubic β-SiC is a low-temperature form [44].

Xingzhong GUO et al. [45], Ceballos-Mendivil et al. [46], Jiang S. et al. [47] and Changhong D. et al. [28] also reported the five characteristic diffraction peaks for β-SiC, 2θ of values 35.6°, 41°, 60°, 71.8° and 75.6° corresponding to (111), (200), (220), (311) and (222) cubic reflections, respectively. In the XRD patterns (Fig. 3), there is a similar observation that the as-prepared SiC powders have diffraction peaks at 2θ values of 35.6°, 41°, 60°, 71.8° and 75.6°, confirming the monopasic β-SiC phase. The XRD results were coherent with this phenomenon of SiC.

Above 1475 °C, the synthesized powders belong predominantly to SiC and no trace of silica was found. The yield of SiC transformation increased with increasing temperature. In the previous studies, it was reported that the reaction yield decreases when reaction temperature is

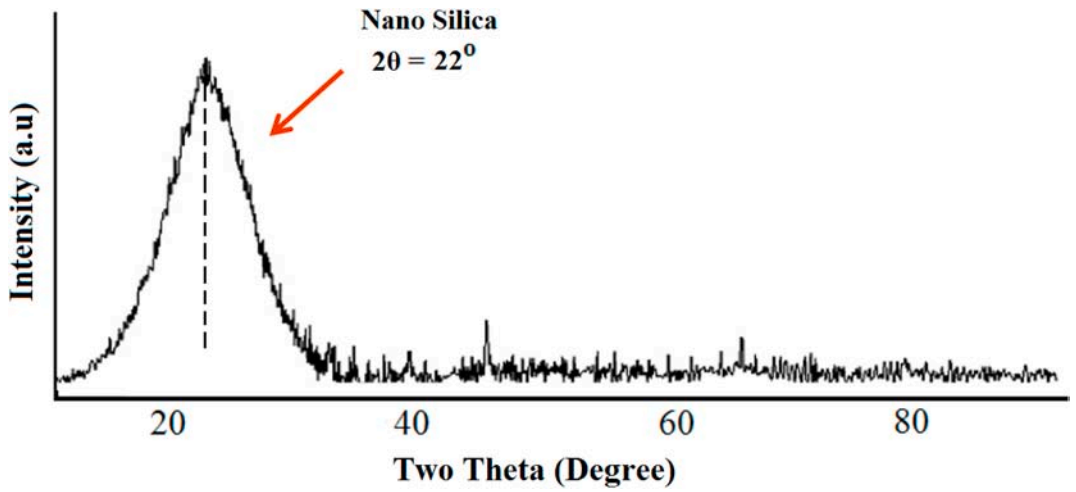

Fig. 2. XRD pattern of SiO_2 after the high energy milling.

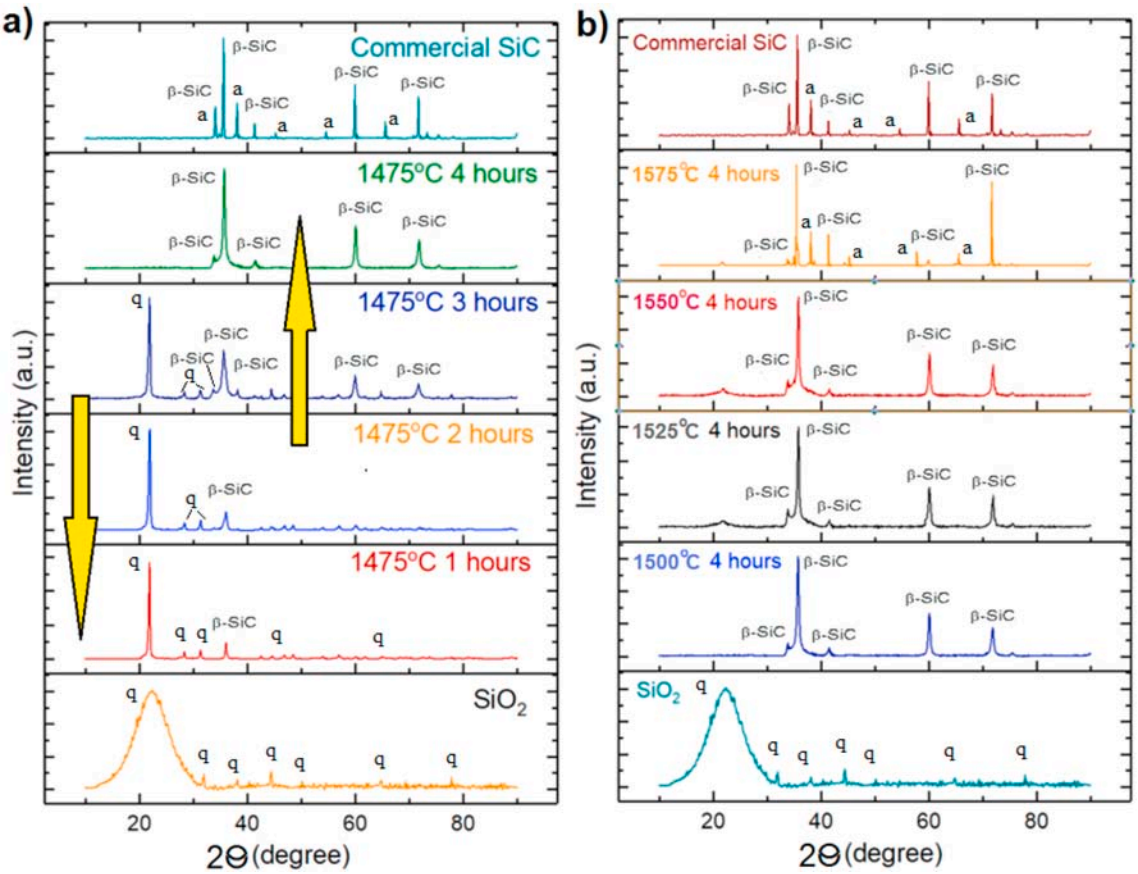

Fig. 3. XRD patterns of the samples synthesized by the CRC processing a) at 1475 °C for 1–4 h and b) at 1500–1575 °C for 4 h. (q: SiO_2, a: α-SiC) β-SiC (JCPDS 29–1129, Quartz (SiO_2) (JCPDS 46–1045), α-SiC (JCPDS 29–1127).

below 1475 °C [20,48]. However, for the samples synthesized at the lowest temperature (1475 °C), the yield of synthesized SiC is similar to commercial SiC. The theoretical reaction temperature of SiC is around 1700 °C. However, in this study, SiC can be synthesized at about 1475 °C because of high milling time that behaves as a mechanical activation.

As a result of mechanical activation of the starting materials, the area of contact between the reactant powder particles increases due to reduction in particle size. This case allows fresh surfaces to come into contact. This effect results in the homogenous mixing the starting materials, which prevents the formation of the secondary phases during the CRC conversion. Therefore, SiC powder product free from undesired secondary phases can be achieved. This result can be seemingly seen for 4 h at 1475 °C in Fig. 3a [42,49,50].

The milling of the starting powders also causes the formation of a large number of lattice defects, high-density of dislocations and free surfaces. These defects quicken the diffusion of SiO_2. As a consequence, while the traditional solid-state reactions for the synthesis of SiC necessitate high temperatures, the solid-state reactions carried out after the mechanical activation will occur at lower temperature. In other words, the high-density defects induced by high energy milling of the

starting powders promote the diffusion process. The particle refinement and the reduction in diffusion distances due to microstructural refinement can at least significantly reduce reaction temperatures [49].

Fig. 3a revealed that the activation energy needed for a reaction between SiO_2 and C to proceed was obtained by heating at temperatures below 1500 °C. There is no noteworthy difference in XRD peaks when the temperature increases from 1475 to 1500–1525 °C. In these temperatures, the unreacted silica remains in amorphous phase with a small peak over 20-30°.

When the reaction temperature increased to 1550 °C, the remained phases transformed to SiC substantially (Fig. 3(b)). Still, other phases were detected in the XRD results. The origin of these undesirable phases can come from contamination due to grinding operations.

3.1.2.2. Seeding effect on synthesizing of the β-SiC phase. The XRD patterns of the powder samples prepared under different conditions (seeding addition, milling conditions) by the CRC reaction at 1475 for 4 h are given in Fig. 4. Long milling time causes the contamination which can be explained by the presence of the $FeSi_2$ phase. It is reported that Fe has a positive effect on the synthesis of SiC by the enhancement of the SiO(g) formation [14]. The second step of SiC formation proceeds readily to the right side of equation (3) when the concentration of $SiO_{(g)}$ increases. But the purity of product decreases with the increasing of impurity elements. The purity of SiC can be enhanced by eliminating $FeSi_2$ and residual SiO_2 using the appropriate leaching method. In Fig. 4, the XRD pattern of unmilled samples shows the amorphous phase peak between 20 and 30°. The seeding effect was investigated by adding commercial SiC about 10%wt. to milled and unmilled samples. When 10%wt. SiC is added, the samples are affected morphologically, but the XRD results are unchanged.

3.2. FTIR results

FTIR is a complement method that provides the spectroscopic information about the chemical groups present in the structure, supporting the data obtained from XRD. The FT-IR spectrum of silica can be seen in Fig. 5. The FTIR investigation is aimed at the determination of the characteristics of activated silica by observing functional groups in silica powder.

In the work of Bock and Su, the IR bands at 377, 465, 800, 950, 1100, and 1190 cm^{-1} were revealed for fused silica. They compared it with the results of vibrational calculations. Crystalline silica (all polymorphs) also had these IR bands. Bock and Su. [51], Tomozawa et al. [52] and Chmel et al. [53] used FTIR to exhibit the changes in amorphous silica.

A strong band at 1136 cm^{-1} is caused by the presence of Si–O–Si (siloxane) stretching. This suggests the partial bonding structure of Si and O atoms at nano size particles. A sharp and intense peak can be easily seen at 891 cm^{-1}. This feature is caused by the Si–O bending vibrations [54,55]. The peak at 457 cm^{-1} is assigned to the Si–O out of plane bending vibrations. The very strong and broad IR band at 1111 cm^{-1} with a shoulder at 1188 cm^{-1} is usually assigned to the longitudinal and transverse modes of the Si–O–Si asymmetric stretching vibrations. The IR band at 956 cm-1 can be assigned to silanol groups [56]. In the FTIR spectrum of SiO_2 (Fig. 5), the absorption band at 1635 cm^{-1} is attributed to H_2O. In general, H_2O is present on the surfaces of SiO_2 particles [57]. In Fig. 5, the FTIR spectrum of SiO_2 agrees well with the spectrum obtained by MusićI S. et al. [56] and Cai X. et al. [58].

The reaction of beta-SiC formation from silica with elevated activity and active carbon is between two solid phases and, in the reaction, silica migrates over the silicon carbide surface to the carbon [59–61]. F. K. van Dijen and R. Metselaar reported that TEM results concerning the reaction mechanism of β-SiC formation from the silica and the carbon seem

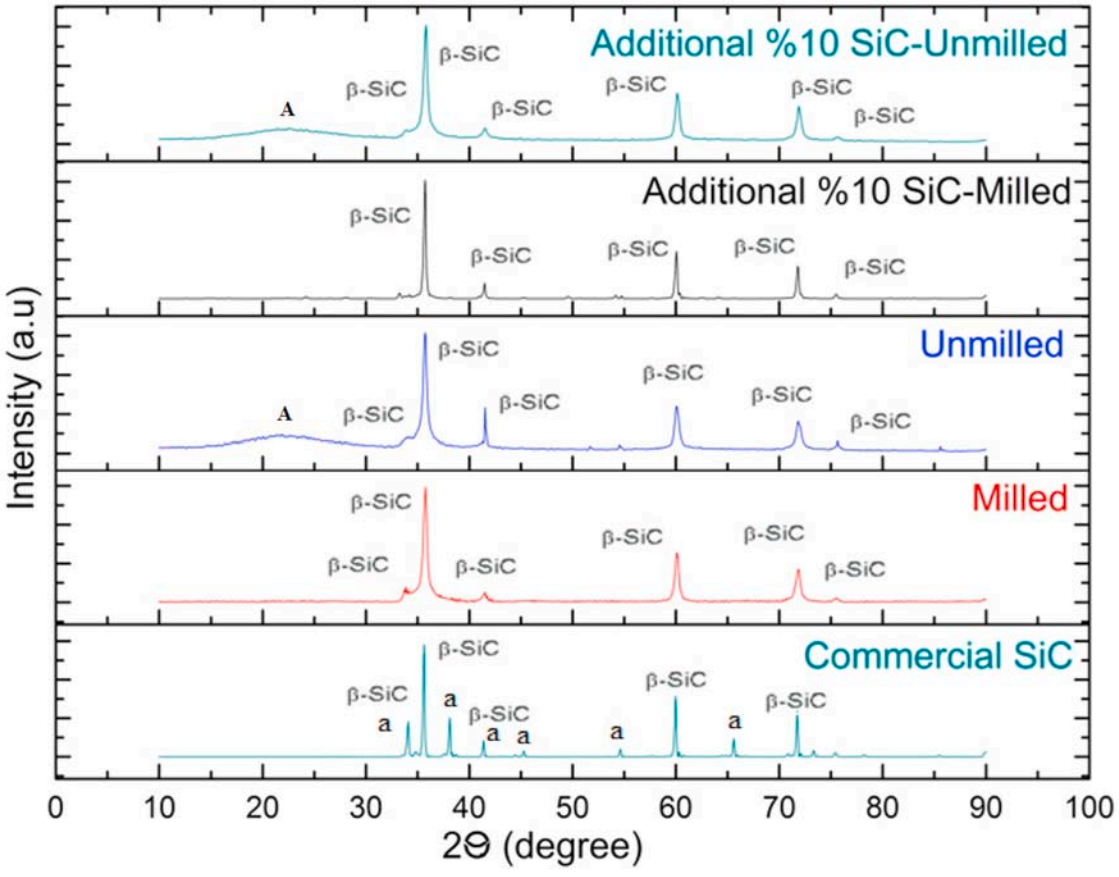

Fig. 4. *XRD patterns of* the samples prepared *in different conditions by* CRC *reaction* at 1475 °C for 4 h.

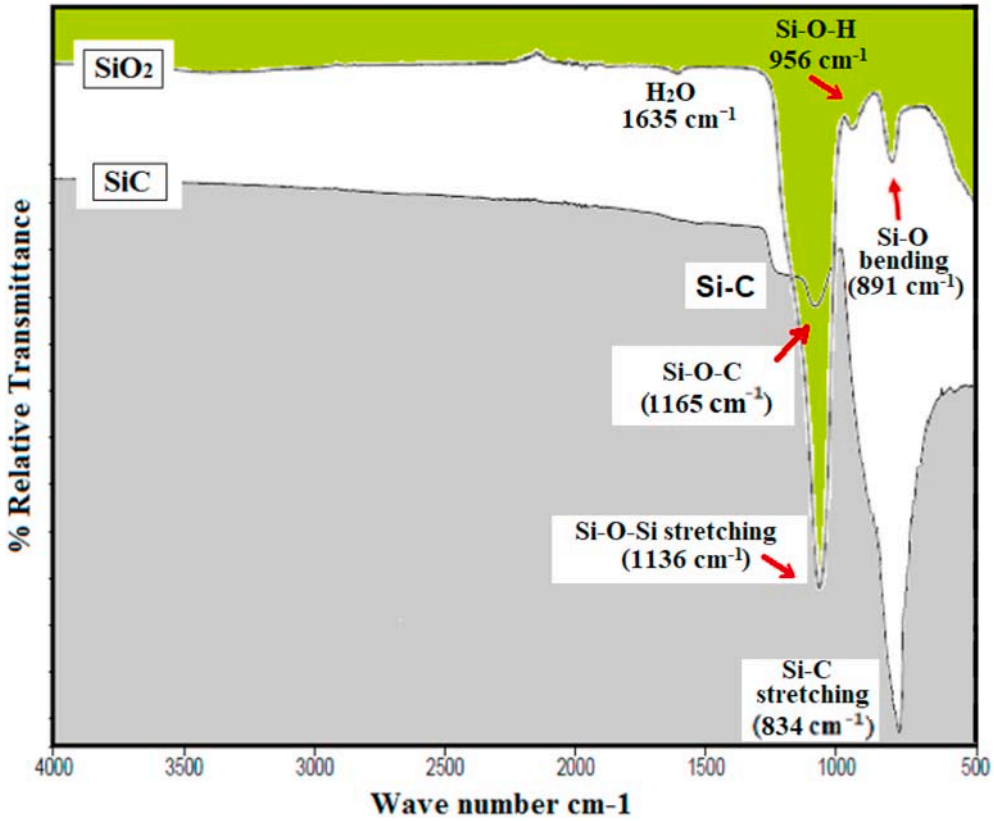

Fig. 5. FT-IR spectrum of mechanical activated SiO_2 and synthesized SiC.

to indicate that the SiO_2 migrates over the silicon carbide particles towards the carbon. The carbothermal reduction and carburization reaction occurs in which the SiO_2 and the C contact. When SiO is first formed, it is thought that all carbon black particles attend the reaction to form SiC crystalline. It should be noted, however, that only carbon particles in contact with SiO_2 react [18].

According to the results found in the literature, the SiC nanowire growth occurs along the [111] direction and the growth mechanism can be attributed to a typical vapor–solid (VS) process. This mechanism was accepted because there were no droplets [59–61].

FT-IR spectroscopy was used to confirm the composition of SiC. As is obviously shown in Fig. 5, the highly intense band that appeared at 834 cm^{-1} can be attributed to Si–C stretching vibrations and this strong and sharp absorption peak corresponds to longitudinal optic (LO) vibration mode [62,63]. The peaks at around 890-950 cm^{-1} are related to the longitudinal optic (LO) vibration mode [62].

The changes in the position of the IR absorption of the Si–C bond may arise due to intrinsic stress. The intrinsic stress in the SiC nanowires may induce strain in the chemical bonds of the IR absorber and cause a shift in the frequency of the IR absorption band. The peak near 950 cm−1 represents the LO stretching Si–C bond; and the peak near 1100 cm−1 correspond to stretching mode Si–O bond [62].

The peak that appeared at 1165 cm^{-1} can be related to the Si–O–C and Si–O–Si stretching vibrations. This weak peak can be attributed to the surface silica on SiC particles. This can be due to the phenomenon of Si to bond as siloxane [64]. The kinetics of SiC–SiO_2 formation can be complex and the siloxane process is a mainly diffusion-controlled mechanism. The pronounced anisotropy of SiC expressed itself by quite different oxidation rates for the various crystallographic faces. The SiC nanowire has a high surface area due to the nano-sized diameter and preferential growth [65–67]. The FT-IR results obtained in the present study for starting silica and synthesized SiC are similar to those reported previous works [62,63,68].

3.3. Scanning electron microscopy

3.3.1. Starting materials after the HMEM

The agglomerate particles are detected in the SEM image, and the particle size varied over 50–100 nm in diameter, with an average diameter of 60 nm. This situation could arise from semi/unstable fresh surfaces after high energy mill. Thus, the mechanical activation can ensure the chemical reactions normally occurring at elevated temperatures. This mechanokinetic situation is similar to that obtained by Boyrazlı M. et al. [40] who reported the reduction in activation energy achieved by the high energy milling process.

The morphology of the quartz mineral is shown in Fig. 6. It is shown that quartz particles are spherical and they are strongly agglomerated. The PSD exhibits homogeneous distribution and characteristics in a narrow range, as shown in Fig. 1. The specific surface area (SSA) of the SiO_2 powder was calculated, approximately, to be equal to at 0.67 m^2/g. The SiO_2 powder is mostly fine and has a great surface area to react with carbon.

Reaction (1) kinetically proceeds very slowly and, so, this reaction occurs in two steps, as solid-solid and solid-gas phase reactions. CO gas which is important for reducing SiO_2 (reaction 4) has been produced during the reaction (2) and (3). Another source of CO gas was produced from the Boudouard reactions (5) spontaneously which had a negative standard Gibbs free energy ($\Delta G = -118.7$ kJ mol^{-1} at 298K). The β-SiC nanopowder particles nucleate heterogeneously on carbon surface by gas-solid state interaction between SiO gas and solid carbon, according to reaction (3). Hovewer, the β-SiC nanowhiskers were mostly a product of the reaction of SiO gas with CO gas (Reaction (6)) via gas-gas phase mechanism.

$$SiO_{2(s)} + CO_{(g)} \rightarrow SiO_{(g)} + CO_{(g)} \quad (4)$$

$$CO_{2(g)} + C_{(s)} \rightarrow 2CO_{(g)} \quad (5)$$

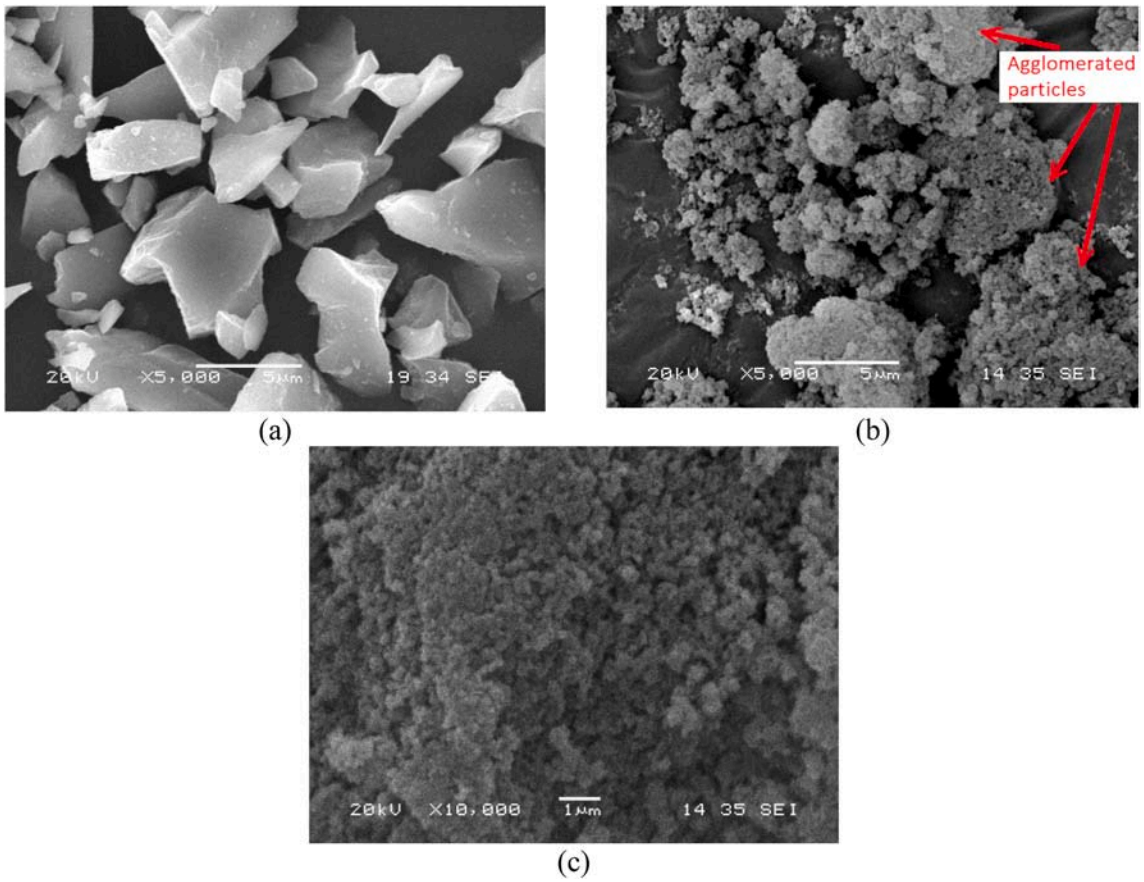

Fig. 6. SEM micrographs of a) as-received SiO_2 powder, agglomerated starting SiO_2 powders after MHEM at magnification of b) X5000 c) X10000.

$$SiO_{(g)} + 3CO_{(g)} \rightarrow SiC_{(s)} + 2CO_{2(g)} \quad (6)$$

3.3.2. After the conversion reaction

SEM can reveal critical morphological details. The morphology of the synthesized SiC particles is shown in Fig. 7. The pure SiC products were obtained from the activated powder by MHEM after CRC at 1475 °C for 4 h. SiC nanowhiskers occurred with the changing reaction time and/or temperature. The nucleation and growth of solid β-SiC nanowhiskers occur during the SiO and CO gas reaction, according to reaction (6). The reaction time was chosen as enough long for the β-SiC nano whiskers growth, on the base of our previous related studies, but the temperature was taken just below the upper boundary of formation of 'β' modification. As minimum synthesis temperature, 1475 °C was selected in this study. When the temperature is above 1475 °C, the development of whisker clusters is observed. It is observed that whiskers formed at increased temperatures are thicker and the thickness reaches maximum values at the maximum test temperature of 1550 °C. It is desirable that SiC has whisker form, which is used to increase fracture toughness. However, in other applications, where compacted and sintered powders are used, the coaxial powders are preferred due to high density. The yield of synthesized SiC is at minimal experimental time of 1 h. The

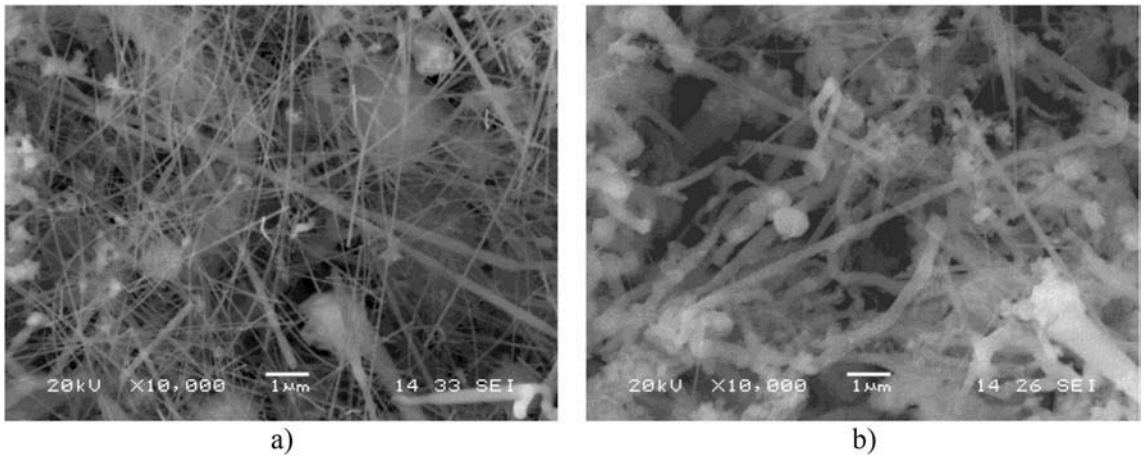

Fig. 7. SEM images of SiC grain morphologies after the reduction and carburization process using a) the activated powder obtained by high energy milling b) the powder composition without any pre-processing at 1475 °C for 4 h.

amount of the conversion from SiO_2 to β-SiC phase increased with the increasing of time and temperature. However, it is observed that powders are coaxially retained at the reaction end. This result led to the growth of whiskers in the form of nucleation over small impurities like Fe in the resulting structure during contamination from the initial powders during grinding. So, it can be said that one of the criteria for coaxial powder production is that the starting powders must be of high purity.

The SEM micrographs reveal that SiC whiskers are of nano-sized diameter when synthesized at 1475 °C for 4 h for the powder prepared with mechanical activation. However, full conversion to SiC is not observed in the samples fired at 1475 °C for 2 h. (Fig. 3a). In fact, it was a clear difference as to the morphology of SiC particles when synthesized for 4 h at 1475 °C for the sample prepared with mechanical activation and without any mechanical activation. There is a meaningful relationship between crystallite diameter of fibrous particle and holding time during CRC process. As can be seen in Figs. 7b and 8b, a clear coarsening in the β-SiC whisker size is observed in CRC process at 1475 °C for 4 h, in comparison with 2 h.

The driving force is a surface area increment, which can improve the reaction ability for the SiC whiskers in the yielded powder, as shown in Fig. 7 (a). The whisker diameter and length change with the preparation process. While the characteristic feature of Fig. 7(a) is the nano-sized whiskers, a conventionally prepared sample in Fig. 7(b) had submicron characteristics. This formation mechanism can be related to more nuclei points for SiC due to more surface area with high energy. This situation can facilitate the development of nano-sized SiC whiskers.

As shown in Fig. 7(a), when the directly prepared batch is converted at 1475 °C, the structure has coarse fibrous SiC grains and the single particle diameter is about 250–300 nm. When the sample obtained after mechanochemical process is converted at 1475 °C, the SiC product contains nano-whiskers with higher aspect ratios and has regular particle morphology and distribution (8–12 μm in length and 50–100 nm in diameter). As seen in Fig. 7(b), the directly prepared sample converted at 1475 °C for 4 h contains inhomogeneous particle morphologies (large and small particles together) compared to Fig. 7 (a).

As shown in Fig. 8(a) and (b), the results of EDS analysis reveal Si and C, components of SiC, and O elements. Generally, the EDS patterns presented in Fig. 7(a) show dominance of Si and C elements and O as a minor element. The presence of oxygen can be attributed to surface silica on SiC. In comparison with Fig. 8(a) and (b) indicates a higher oxygen amount that means the presence of unreacted silica. It can be concluded that the difference between the oxygen peaks in Fig. 8a and b confirms that there is a better conversion of SiO_2 to SiC for the powder obtained by using the MHEM system with the CRC processing. The increase in the specific area of the powders (due to the MHEM) causes the formation of a large density of finer crystallites in the resulting materials. SEM micrograph of the CRC resulting sample in Fig. 7a is evident for this mechanism, in contrast to Fig. 7b sample as [41,42]. These results are consistent with the XRD and SEM analyses results in the present study. The solid-state reactions initiated by mechanical activation in high energy ball mills appeared to be a good choice for the ultrafine β-SiC powder preparation.

3.3.3. *The effect of synthesizing temperature on the morphology of SiC particles*

Silicon carbide fibre/whisker can be single, polycrystalline or non-crystalline that are cylindrical in shape [68]. In addition, they can be influenced by the synthesis process and its parameters. The length and diameter of these SiC whiskers can be changed, and the aspect ratio is usually above 3 [69].

A correlation is obtained between the change of the diameter of β-SiC fibrous particles and temperature in CRC process as shown in Fig. 9. The diameter of SiC particles is in the range 50–100 nm at 1475 °C for 4 h. The SEM measurement showed a narrow size distribution and an almost homogeneous diameter. At 1525 °C for 4 h, the diameter increases 80–350 nm. The SiC fibrous particle coarsening and widening diameter (df) range were clarified with a temperature increase by 50 °C. As for the 1550 °C, the diameter became even more wider and fibrous SiC particles reach maximum of 700 nm in the crystallite diameter. It should be noted

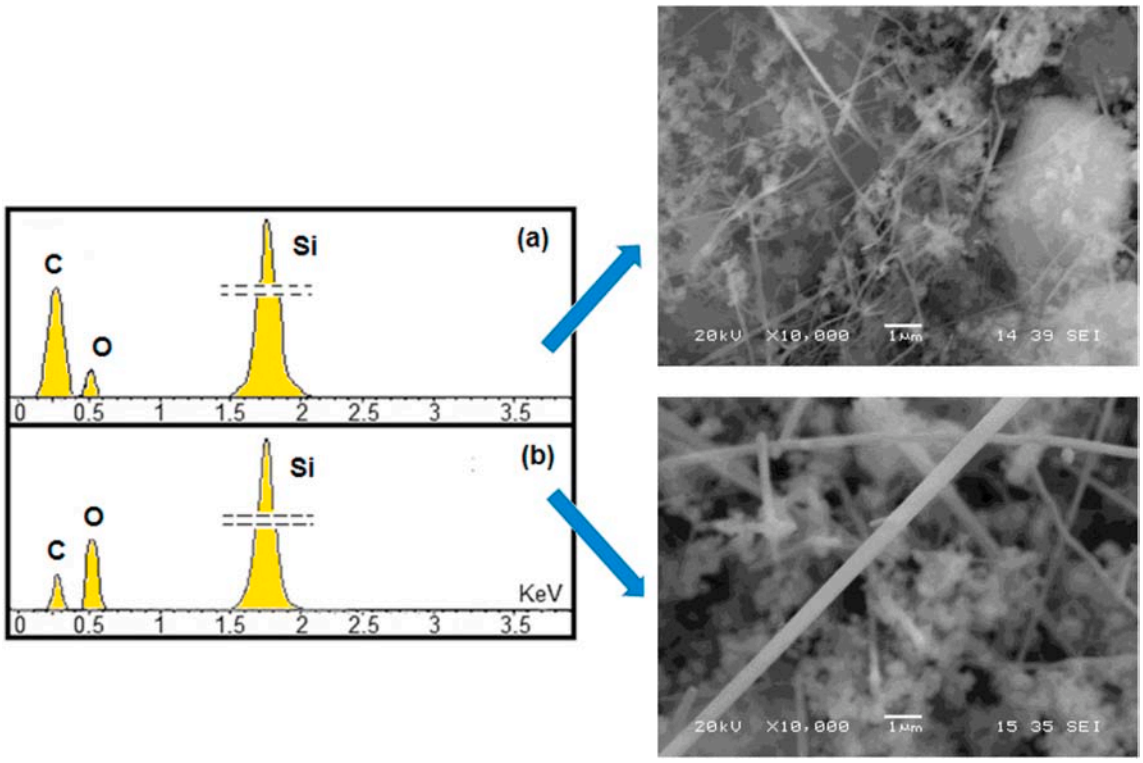

Fig. 8. SEM image and EDS analysis of a) the sample prepared with mechanical activation b) the sample prepared without mechanical activation converted at 1475 °C for 2 h.

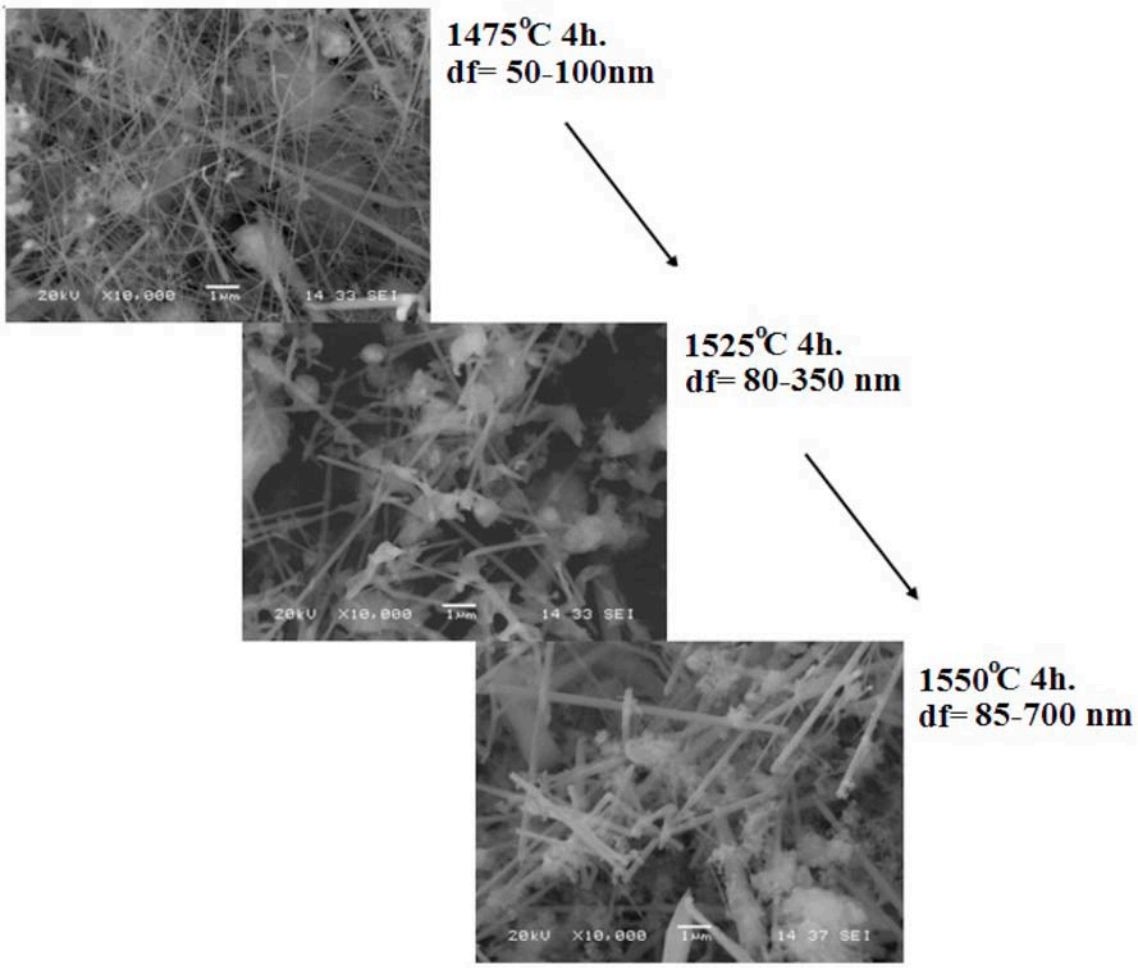

Fig. 9. Change of SiC fibrous particle diameter as a function of temperature. All samples were prepared by the MHEM. df is the diameter of SiC fibrous particle.

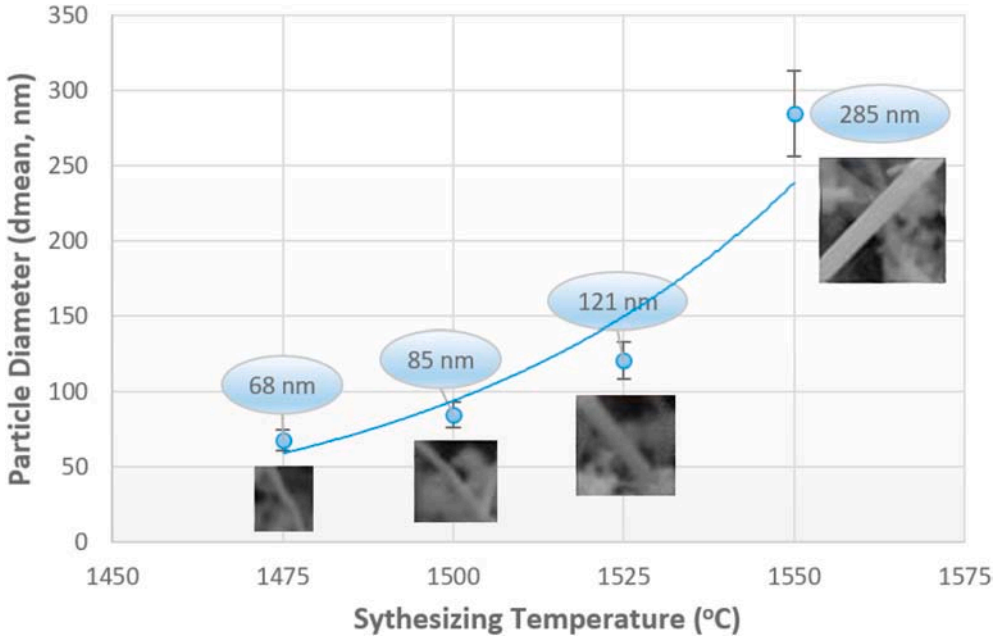

Fig. 10. Mean particle diameter as a function of temperature. Mean particle diameter (dmean) was calculated by measuring the diameter of 20 particles for each value.

that the fibrous morphology of SiC particles homogeneously coarsened throughout the powder with the increase in the temperature.

The holding temperature increase results in coarsening of SiC whisker size. As shown in Fig. 10, the mean diameter size change in the range from 68 to 285 nm.

4. Conclusion

The SiC nanowires 50–100 nm in diameter were synthesized by the carbothermal reduction and carburization method at relatively low temperatures from amorphous silica particles obtained with the designed pre-mechanical preparation process (MHEM).

- The XRD results confirmed the full transformation reaction from SiO_2 to β-SiC, accompanied by decreasing the amount of the remaining silica.
- Characterization indicates that SiC obtained is composed of cubic type SiC (β-SiC).
- Synthesis of SiC is not carried out if the holding time is below the threshold time.
- A preferred orientation was observed in growth direction after the CRC processing.
- Ultrafine fibrous and homogeneously distributed particles were obtained by using the MHEM system with the CRC processing.
- The EDS analyses were used to illustrate the influence of the MHEM treatment on SiC composition.
- The EDS analysis confirmed that the resulting fibrous grains were silicon carbide nano-rods.
- SEM micrographs and size measurement results pointed out an obvious increase in diameter of SiC crystallites as a function of temperature.
- FTIR results indicate that the powder chemistry was fairly affected by the milling conditions before synthesizing.
- It was determined that a major contribution to the conversion and crystallite diameter change was due to the behaviour of amorphous phase obtained after high energy milling.
- The carbothermal reduction and carburization process were performed in a tube furnace with atmosphere control, resulting in the β-SiC formation, accompanied by a decrease in the plateau temperature (at 1475 °C for 4 h). Compared to the previous studies, production of ultrafine β-SiC particles was achieved without any catalysis addition and at a low temperature.
- With the aforementioned reasons, the batch preparation process for the CRC has a main effect on the yield powder morphology. This influences the final ceramic product features.
- The solid-state reactions initiated by mechanical activation in high energy ball mills appeared to be a good choice for β-SiC nano-powder preparation.

CRediT authorship contribution statement

Engin Kocaman: Investigation, Software, Validation, Visualization. **Fatih Çalışkan:** Methodology, Software, Formal analysis, Writing - review & editing, Supervision.

Declaration of competing interest

The authors declare that they have no known competing financial interests or personal relationships that could have appeared to influence the work reported in this paper.

Appendix A. Supplementary data

Supplementary data to this article can be found online at https://doi.org/10.1016/j.matchemphys.2020.123716.

References

[1] G.W. Meng, Z. Cui, L.D. Zhang, F. Phillipp, Growth and characterization of nanostructured β-SiC via carbothermal reduction of SiO2 xerogels containing carbon nanoparticles, J. Cryst. Growth 209 (2000) 801–806, https://doi.org/10.1016/S0022-0248(99)00435-2.

[2] B. Babić, D. Bučevac, A. Radosavljević-Mihajlović, A. Došen, J. Zagorac, J. Pantić, B. Matović, New manufacturing process for nanometric SiC, J. Eur. Ceram. Soc. 32 (2012) 1901–1906, https://doi.org/10.1016/j.jeurceramsoc.2011.08.023.

[3] K. Niihara, New design concept of structural ceramics, J. Ceram. Soc. Japan 99 (1991) 974–982, https://doi.org/10.2109/jcersj.99.974.

[4] D. Chaira, B.K. Mishra, S. Sangal, Synthesis and characterization of silicon carbide by reaction milling in a dual-drive planetary mill, 460–461, Mater. Sci. Eng., A (2007) 111–120, https://doi.org/10.1016/j.msea.2007.01.080.

[5] J.-H. Eom, Y.-W. Kim, S. Raju, Processing and properties of macroporous silicon carbide ceramics: a review, J. Asian Ceram. Soc 1 (2013) 220–242, https://doi.org/10.1016/j.jascer.2013.07.003.

[6] R. Wu, K. Zhou, C.Y. Yue, J. Wei, Y. Pan, Recent progress in synthesis, properties and potential applications of SiC nanomaterials, Prog. Mater. Sci. 72 (2015) 1–60, https://doi.org/10.1016/j.pmatsci.2015.01.003.

[7] J. Prakash, R. Venugopalan, B.M. Tripathi, S.K. Ghosh, J.K. Chakravartty, A. K. Tyagi, Chemistry of one dimensional silicon carbide materials: principle, production, application and future prospects, Prog. Solid State Chem. 43 (2015) 98–122, https://doi.org/10.1016/j.progsolidstchem.2015.06.001.

[8] A. Najafi, F.G. Fard, H.R. Rezaie, N. Ehsani, Synthesis and characterization of SiC nano powder with low residual carbon processed by sol-gel method, Powder Technol. 219 (2012) 202–210, https://doi.org/10.1016/j.powtec.2011.12.045.

[9] T.W. Cheng, C.W. Hsu, A study of silicon carbide synthesis from waste serpentine, Chemosphere 64 (2006) 510–514, https://doi.org/10.1016/j.chemosphere.2005.11.018.

[10] B.M. Moshtaghioun, A. Monshi, M.H. Abbasi, F. Karimzadeh, A study on the effects of silica particle size and milling time on synthesis of silicon carbide nanoparticles by carbothermic reduction, Int. J. Refract. Metals Hard Mater. 29 (2011) 645–650, https://doi.org/10.1016/j.ijrmhm.2011.04.009.

[11] S. Dhage, H.C. Lee, M.S. Hassan, M.S. Akhtar, C.Y. Kim, J.M. Sohn, K.J. Kim, H. S. Shin, O.B. Yang, Formation of SiC nanowhiskers by carbothermic reduction of silica with activated carbon, Mater. Lett. 63 (2009) 174–176, https://doi.org/10.1016/j.matlet.2008.09.056.

[12] A.S. Mukasyan, Combustion synthesis of silicon carbide, in: R. Gerhardt (Ed.), Prop. Appl. Silicon Carbide, IntechOpen, Rijeka, 2011, https://doi.org/10.5772/15620.

[13] F. Çalışkan, A. Demir, Z. Tatlı, Fabrication of Si3N4 preforms from Si3N4 produced via CRN technique, J. Porous Mater. 20 (2013) 1501–1507, https://doi.org/10.1007/s10934-013-9736-9.

[14] B.M. Moshtaghioun, R. Poyato, F.L. Cumbrera, S. de Bernardi-Martin, A. Monshi, M.H. Abbasi, F. Karimzadeh, A. Dominguez-Rodriguez, Rapid carbothermic synthesis of silicon carbide nano powders by using microwave heating, J. Eur. Ceram. Soc. 32 (2012) 1787–1794, https://doi.org/10.1016/j.jeurceramsoc.2011.12.021.

[15] D.F. Carroll, A.W. Weimer, S.D. Dunmead, G.A. Eisman, J.H. Hwang, G.A. Cochran, D.W. Susnitzky, D.R. Beaman, C.L. Conner, Carbothermally prepared nanophase SIC/Si3N4 composite powders and densified parts, 1997, p. 4.

[16] H.-P. Martin, R. Ecke, E. Müller, Synthesis of nanocrystalline silicon carbide powder by carbothermal reduction, J. Eur. Ceram. Soc. 18 (1998) 1737–1742, https://doi.org/10.1016/S0955-2219(98)00094-6.

[17] W. Wesch, Silicon carbide: synthesis and processing, Nucl. Instrum. Methods Phys. Res. 116 (1996) 305–321, https://doi.org/10.1016/0168-583X(96)00065-1.

[18] F.K. van Dijen, U. Vogt, The chemistry of the carbothermal synthesis of α-Si3N4: reaction mechanism, reaction rate and properties of the product, J. Eur. Ceram. Soc. 10 (1992) 273–282, https://doi.org/10.1016/0955-2219(92)90082-O.

[19] B. Matovic, A. Saponjic, A. Devecerski, M. Miljkovic, Fabrication of SiC by carbothermal-reduction reactions of diatomaceous earth, J. Mater. Sci. 42 (2007) 5448–5451, https://doi.org/10.1007/s10853-006-0780-6.

[20] E. Kocaman, Karbotermik RedüksiyonYöntemiyle Silikadan Tek Fazli Alfa Si3N4 Ve Çift Fazli Si3N4-SiC Teknolojik Seramik Tozlarinin Sentezi Ve Karakterizasyonu, 2016.

[21] L.C. De Jonghe, M.N. Rahaman, in: S. Sōmiya, F. Aldinger, N. Claussen, R. M. Spriggs, K. Uchino, K. Koumoto, M.B.T. H, A.C. Kaneno (Eds.), Chapter 4 - 4.1 Sintering of Ceramics, Academic Press, Oxford, 2003, pp. 187–264, https://doi.org/10.1016/B978-012654640-8/50006-7.

[22] S. Shahrestani, M.C. Ismail, S. Kakooei, M. Beheshti, Effect of additives on slip casting rheology, microstructure and mechanical properties of Si3N4/SiC composites, Ceram. Int. 46 (2020) 6182–6190, https://doi.org/10.1016/j.ceramint.2019.11.085.

[23] S. Xu, G. Qiao, H. Wang, D. Li, T. Lu, Preparation of aligned silicon carbide whiskers from porous carbon foam by silicon thermal evaporation, Mater. Lett. 62 (2008) 4549–4551, https://doi.org/10.1016/j.matlet.2008.08.038.

[24] H.X. Zhang, P.X. Feng, V. Makarov, B.R. Weiner, G. Morell, Synthesis of nanostructured SiC using the pulsed laser deposition technique, Mater. Res. Bull. 44 (2009) 184–188, https://doi.org/10.1016/j.materresbull.2008.03.020.

[25] J. Li, T. Shirai, M. Fuji, Silicon carbide and its nanostructure, Adv. Ceram. Res. Cent. Annu. Rep 3 (2014) 5–10.

[26] J. Li, J. Tian, L. Dong, Synthesis of SiC precursors by a two-step sol–gel process and their conversion to SiC powders, J. Eur. Ceram. Soc. 20 (2000) 1853–1857, https://doi.org/10.1016/S0955-2219(00)00055-8.

[27] B. Zhang, J. Li, J. Sun, S. Zhang, H. Zhai, Z. Du, Nanometer silicon carbide powder synthesis and its dielectric behavior in the GHz range, J. Eur. Ceram. Soc. 22 (2002) 93–99, https://doi.org/10.1016/S0955-2219(01)00248-5.
[28] D. Changhong, Z. Xianpeng, Z. Jinsong, Y. Yongjin, C. Lihua, X. Fei, The synthesis of ultrafine SiC powder by the microwave heating technique, J. Mater. Sci. 32 (1997) 2469–2472, https://doi.org/10.1023/A:1018573611420.
[29] J. Li, T. Shirai, M. Fuji, Direct synthesis of one-dimensional silicon carbide nanostructures on graphite by pyrolysis of rice husks, J. Ceram. Soc. Japan 121 (2013) 211–214, https://doi.org/10.2109/jcersj2.121.211.
[30] W.Z. Zhu, M. Yan, Effect of gas flow rate on ultrafine SiC powders synthesized through chemical vapor deposition in the SiH{sub 4}-C{sub 2}H{sub 4}-H{sub 2} system, Scripta Mater. 39 (1998), https://doi.org/10.1016/S1359-6462(98)00372-8.
[31] M. Sopicka-Lizer, in: M.B.T.-H.-E.B.M. Sopicka-Lizer (Ed.), 8 - Mechanochemical Processing of Non-oxide Systems with Highly Covalent Bonds, Woodhead Publishing, 2010, pp. 167–192, https://doi.org/10.1533/9781845699444.2.167.
[32] F. Çaliçkan, E. Kocaman, T. Tehçi, Synthesis of B4C-SiC in-situ composite powders through carbothermic reactions, Acta Phys. Pol. A 134 (2018) 113–115, https://doi.org/10.12693/APhysPolA.134.113.
[33] F. Calışkan, H. Güngördü, Z. Tatlı, A. Demir, E. Antika, Y, The Design of New Type Mixer for More Efficient Powder Mixing, 2017. Elazığ-Turkey.
[34] G. Nallathambi, T. Ramachandran, V. Rajendran, R. Palanivelu, Effect of silica nanoparticles and BTCA on physical properties of cotton fabrics, Mater. Res. 14 (2011) 552–559, https://doi.org/10.1590/S1516-14392011005000086.
[35] U. Zulfiqar, T. Subhani, S.W. Husain, Synthesis and characterization of silica nanoparticles from clay, J. Asian Ceram. Soc 4 (2016) 91–96, https://doi.org/10.1016/j.jascer.2015.12.001.
[36] F. Yves, B. Jerome, XRD: Structural Analysis List. https://www.list.lu/fileadmin//files/Event/sites/tudor/files/event/4_Presentation_Dr_Yves_Fleming.pdf, 2020.
[37] C. Suryanarayana, Mechanical alloying and milling, Prog. Mater. Sci. 46 (2001) 1–184, https://doi.org/10.1016/S0079-6425(99)00010-9.
[38] B.D. Cullity, S.R. Stock, Elements of X-Ray Diffraction, third ed., Prentice-Hall, New York, 2001.
[39] K. Yildiz, T. Tunç Parlak, F. Apaydin, Effects of mechanical activation on the structure of nickeliferous laterite, Acta Phys. Pol. Ser. A 123 (2013) 349.
[40] Mustafa Boyrazlı, Elif Arancı Öztürk, Yunus Emre Benkli, The effect of the grinding time on the mechanical activation of MnO2 ore and tea plant waste carbonization product, J. Phys. Sci. Appl. 7 (2017) 59–65, https://doi.org/10.17265/2159-5348/2017.04.007.
[41] R. Ashiri, A. Heidary Moghadam, R. Ajami, Obtaining the highly pure barium titanate nanocrystals by a new approach, J. Alloys Compd. 648 (2015) 265–268, https://doi.org/10.1016/j.jallcom.2015.06.234.
[42] A. Moghtada, A. Heidary Moghadam, R. Ashiri, Tetragonality enhancement in BaTiO3 by mechanical activation of the starting BaCO3 and TiO2 powders: characterization of the contribution of the mechanical activation and postmilling calcination phenomena, Int. J. Appl. Ceram. Technol. 15 (2018) 1518–1531, https://doi.org/10.1111/ijac.13019.
[43] J.L. Gary, G. Fernande (Eds.), Mössbauer Spectroscopy Applied to Magnetism and Materials Science, first ed., Springer, Boston, MA, 1993 https://doi.org/10.1007/978-1-4899-2409-4.
[44] S. Føreland, E. Bye, B. Bakke, W. Eduard, Exposure to fibres, crystalline silica, silicon carbide and sulphur dioxide in the Norwegian silicon carbide industry, Ann. Occup. Hyg. 52 (2008) 317–336, https://doi.org/10.1093/annhyg/men029.
[45] X. Guo, L. Zhu, W. Li, H. Yang, Preparation of SiC powders by carbothermal reduction with bamboo charcoal as renewable carbon source, J. Adv. Ceram 2 (2013) 128–134, https://doi.org/10.1007/s40145-013-0050-4.
[46] L.G. Ceballos-Mendivil, R.E. Cabanillas-López, J.C. Tánori-Córdova, R. Murrieta-Yescas, C.A. Pérez-Rábago, H.I. Villafán-Vidales, C.A. Arancibia-Bulnes, C. A. Estrada, Synthesis of silicon carbide using concentrated solar energy, Sol. Energy 116 (2015) 238–246, https://doi.org/10.1016/j.solener.2015.04.006.
[47] S. Jiang, S. Gao, J. Kong, X. Jin, D. Wei, D. Li, P. Xing, Study on the synthesis of β-SiC nanoparticles from diamond-wire silicon cutting waste, RSC Adv. 9 (2019) 23785–23790, https://doi.org/10.1039/C9RA03383A.
[48] F. Çalışkan, E. Kocaman, S. Cömert, Synthesis of the in-situ Si3N4-SiC composite nano powders by carbothermal reduction, Acta Phys. Pol. A 131 (2017) 601–605, https://doi.org/10.12693/APhysPolA.131.601.
[49] R. Ashiri, Analysis and characterization of phase evolution of nanosized BaTiO3 powder synthesized through a chemically modified sol-gel process, Metall. Mater. Trans. A 43 (2012) 4414–4426, https://doi.org/10.1007/s11661-012-1242-1.
[50] R. Ashiri, On the solid-state formation of BaTiO3 nanocrystals from mechanically activated BaCO3 and TiO2 powders: innovative mechanochemical processing{,} the mechanism involved{,} and phase and nanostructure evolutions, RSC Adv. 6 (2016) 17138–17150, https://doi.org/10.1039/C5RA22942A.
[51] J.A.N. Bock, G.-J. Su, Interpretation of the infrared spectra of fused silica, J. Am. Ceram. Soc.. 53 (n.d.) 69–73. doi:10.1111/j.1151-2916.1970.tb12012.x.
[52] M. Tomozawa, J.W. Hong, S.R. Ryu, Infrared (IR) investigation of the structural changes of silica glasses with fictive temperature, J. Non-Cryst. Solids 351 (2005) 1054–1060, https://doi.org/10.1016/j.jnoncrysol.2005.01.017.
[53] A. Chmel, E.K. Mazurina, V.S. Shashkin, Vibrational spectra and deffect structure of silica prepared by non-organic sol-gel process, J. Non-Cryst. Solids 122 (1990) 285–290, https://doi.org/10.1016/0022-3093(90)90993-V.
[54] O. Mardiana, Haryadi, production and application of olivine nano-silica in concrete, IOP Conf. Ser. Mater. Sci. Eng. 204 (2017), https://doi.org/10.1088/1757-899X/204/1/012008.
[55] B. Shokri, M.A. Firouzjah, S.I. Hosseini, FTIR analysis of silicon dioxide thin film deposited by metal organic-based PECVD, Proc. 19th Int. Plasma Chem. Soc (2009) 1–4. www.ispc-conference.org.
[56] S. Musić, N. Filipović-Vinceković, L. Sekovanić, Precipitation of amorphous SiO2 particules and their properties, Brazilian J. Chem. Eng 28 (2011) 89–94, https://doi.org/10.1590/S0104-66322011000100011.
[57] Y. Liang, J. Ouyang, H. Wang, W. Wang, P. Chui, K. Sun, Synthesis and characterization of core–shell structured SiO2@YVO4:Yb3+,Er3+ microspheres, Appl. Surf. Sci. 258 (2012) 3689–3694, https://doi.org/10.1016/j.apsusc.2011.12.006.
[58] X. Cai, R.Y. Hong, L.S. Wang, X.Y. Wang, H.Z. Li, Y. Zheng, D.G. Wei, Synthesis of silica powders by pressured carbonation, Chem. Eng. J. 151 (2009) 380–386, https://doi.org/10.1016/j.cej.2009.03.060.
[59] J.B. Hannon, S. Kodambaka, F.M. Ross, R.M. Tromp, The influence of the surface migration of gold on the growth of silicon nanowires, Nature 440 (2006) 69, https://doi.org/10.1038/nature04574.
[60] S. Hofmann, R. Sharma, C.T. Wirth, F. Cervantes-Sodi, C. Ducati, T. Kasama, R. E. Dunin-Borkowski, J. Drucker, P. Bennett, J. Robertson, Ledge-flow-controlled catalyst interface dynamics during Si nanowire growth, Nat. Mater. 7 (2008) 372, https://doi.org/10.1038/nmat2140.
[61] P. Hu, S. Dong, X. Zhang, K. Gui, G. Chen, Z. Hu, Synthesis and characterization of ultralong SiC nanowires with unique optical properties, excellent thermal stability and flexible nanomechanical properties, Sci. Rep. 7 (2017) 1–10, https://doi.org/10.1038/s41598-017-03588-x.
[62] D. Abdurazik, Fourier Transform Infrared Spectroscopy (FTIR) Analysis of Silicon Carbide Nanowires by, (n.d.).
[63] V. Chung, S. Tony, C. Hong, C. Chuan, B. Ying, S. Chandra, Effective synthesis of silicon carbide nanotubes by microwave heating of blended silicon dioxide and multi-walled carbon, Nanotube 20 (2017) 1658–1668.
[64] M. Reza-E-Rabby, S. Jeelani, V. Rangari, Structural analysis of polyhedral oligomeric silsesquioxane coated SiC nanoparticles and their applications in thermoset polymers, J. Nanomater. 2015 (2015) 13.
[65] V. Presser, K.G. Nickel, Silica on silicon carbide, Crit. Rev. Solid State Mater. Sci. 33 (2008) 1–99, https://doi.org/10.1080/10408430701718914.
[66] M. Bechelany, J.L. Riesterer, A. Brioude, D. Cornu, P. Miele, Rayleigh instability induced SiC/SiO2 necklace like nanostructures, CrystEngComm 14 (2012) 7744–7748, https://doi.org/10.1039/C2CE25636C.
[67] G.T. Burns, R.B. Taylor, Y. Xu, A. Zangvil, G.A. Zank, High-temperature chemistry of the conversion of siloxanes to silicon carbide, Chem. Mater. 4 (1992) 1313–1323, https://doi.org/10.1021/cm00024a035.
[68] H. Liu, Z. Huang, J. Huang, M. Fang, Y.-G. Liu, X. Wu, Thermal evaporation synthesis of SiC/SiO nanochain heterojunctions and their photoluminescence properties, J. Mater. Chem. C 2 (2014) 7761–7767, https://doi.org/10.1039/c4tc01391c.
[69] K. Rödelsperger, B. Brückel, The carcinogenicity of WHO fibers of silicon carbide: SiC whiskers compared to cleavage fragments of granular SiC, Inhal. Toxicol. 18 (2006) 623–631, https://doi.org/10.1080/08958370600742987.